Atmos. Chem. Phys., 11, 6515–6527, 2011
www.atmos-chem-phys.net/11/6515/2011/
doi:10.5194/acp-11-6515-2011

Atmospheric Chemistry and Physics

A multi-sensor upper tropospheric ozone product (MUTOP) based on TES Ozone and GOES water vapor: derivation

S. R. Felker[1], J. L. Moody[1], A. J. Wimmers[2], G. Osterman[3], and K. Bowman[3]

[1]University of Virginia, Charlottesville, VA, USA
[2]Cooperative Institute for Meteorological Satellite Studies, Madison, WI, USA
[3]NASA Jet Propulsion Laboratory, Pasadena, CA, USA

Received: 5 June 2010 – Published in Atmos. Chem. Phys. Discuss.: 10 December 2010
Revised: 15 April 2011 – Accepted: 9 June 2011 – Published: 8 July 2011

Abstract. The Tropospheric Emission Spectrometer (TES), a hyperspectral infrared instrument on the Aura satellite, retrieves a vertical profile of tropospheric ozone. However, polar-orbiting instruments like TES provide limited nadir-view coverage. This work illustrates the value of these observations when taken in context with geostationary imagery describing synoptic-scale weather patterns. The goal of this study is to create map-view products of upper troposphere (UT) ozone through the integration of TES ozone measurements with two synoptic dynamic tracers of stratospheric influence: specific humidity derived from the GOES Imager water vapor absorption channel, and potential vorticity (PV) from an operational forecast model. As a mixing zone between tropospheric and stratospheric reservoirs, the upper troposphere (UT) exhibits a complex chemical makeup. Determination of ozone mixing ratios in this layer is especially difficult without direct in situ measurement. However, it is well understood that UT ozone is correlated with dynamical tracers like low specific humidity and high potential vorticity. Blending the advantages of two remotely sensed quantities (GOES water vapor and TES ozone) is at the core of the Multi-sensor Upper Tropospheric Ozone Product (MUTOP).

Our results suggest that 72 % of TES-observed UT ozone variability can be explained by its correlation with dry air and high PV. MUTOP reproduces TES retrievals across the GOES-West domain with a root mean square error (RMSE) of 18 ppbv (part per billion by volume). There are several advantages to this multi-sensor derived product approach: (1) it is calculated from two operational fields (GOES specific humidity and GFS PV), so maps of layer-average ozone can be created and used in near real-time; (2) the product provides the spatial resolution and coverage of a geostationary image as it depicts the variable distribution of ozone in the UT; and (3) the 6 h temporal resolution of the derived product imagery allows for the visualization of rapid movement of this dynamically-driven ozone, as illustrated in the animation Supplement. This paper presents the scientific basis and methodology behind the creation of this unique ozone product, as well as a statistical comparison of the derived product to an evaluation dataset of coincident TES observations.

Correspondence to: S. R. Felker
(srfelker@gmail.com)

1 Introduction

Ozone in the upper troposphere (UT) continues to receive great attention in the scientific literature due to its role in clear-sky radiative forcing (Wang et al., 1995; Gauss et al., 2003; Worden et al., 2007a), its potential downstream movement into populated boundary layers (Cooper et al., 2004a; Hudman et al., 2004), and its rather unique position within the mixing zone between stratospheric and tropospheric reservoirs (Shepherd, 2002; Bowman et al., 2007; Fairlie et al., 2007). Stratosphere to troposphere transport is an important source of ozone for the UT, and a variety of methods have been employed to identify dynamical features associated with ozone exchange. Stohl et al. (2003) provide an excellent review of stratosphere troposphere exchange (STE). It is generally accepted that tropopause folding occurs in association with significant latitudinal displacements of the tropopause along sloping isentropic surfaces, conditions that occur in the vicinity of the polar and subtropical jet stream, and in association with cutoff lows. The literature also contains many references to the value of potential vorticity and upper tropospheric specific humidity as tracers of stratospheric ozone enhancements in the upper troposphere. Air in the extratropical troposphere is stirred quasi-adiabatically by large-scale transitory cyclones and anticyclones, and stratospheric signatures are reasonably well preserved by these quasi-conservative tracers. In this paper, we

seek to characterize the variations in ozone associated with time-varying synoptic dynamic conditions in the upper troposphere.

Although there are various methods for measuring ozone mixing ratios in the UT (e.g., ozonesondes, differential absorption LiDAR (DIAL), and in situ aircraft measurements), all of these provide very limited spatial and temporal coverage. With the advent of hyper-spectral satellite remote sensing instruments such as the Tropospheric Emission Spectrometer (TES), it is now possible to retrieve a more extensive dataset providing a better perspective of UT ozone. The TES instrument is a high-resolution infrared Fourier transform spectrometer with a nadir view footprint of 5.3×8.5 km (Beer et al., 2001; Beer, 2006; Hilsenrath et al., 2006). TES measures ozone from onboard the NASA Aura satellite ~705 km above the earth in a sun-synchronous polar orbit. One of the main proposed goals of the TES mission is to provide a global view of the vertically resolved ozone distribution within the troposphere (Beer, 2006). One current product of TES is the daily ozone map, available at specific levels (Fig. 1 shows a typical image at 316 hPa). While this type of gridded image product can be useful as a quick look, it is limited in its spatial and temporal resolution, and is unable to characterize relationships between observed ozone enhancements and dynamic meteorological conditions in the UT. Our goal is to derive a more synoptic representation of UT ozone. These results are compared with previous efforts to employ satellite observations to describe ozone variability in the troposphere; efforts based on a range of ozone remote sensing instruments and producing tropospheric column residual maps of ozone. These comparisons help establish that the product presented here is unique in resolving even mesoscale features in the upper troposphere on a sub-daily time-scale, providing a good measure of the correspondence of ozone with rapidly changing meteorological conditions.

1.1 Synoptic dynamics and upper tropospheric ozone tracers

The primary goal of this study is to illustrate the correlation between TES ozone and geostationary observations of UT aridity (low specific humidity), and to exploit this correlation to produce a derived product image: a map view of the upper troposphere that effectively captures synoptic dynamic variations in ozone. A secondary goal is to validate the product, MUTOP, against in situ ozonesonde data; this is presented in a separate manuscript (Moody et al., 2011). Past validation studies have examined correlations between large data sets of TES-observed ozone profiles and ozonesonde, DIAL, or aircraft spiral ozone profiles without any significant consideration of the coincident large-scale weather patterns. By comparison, this study is focused on whether, and how well, TES-observed UT ozone responds to changes in the synoptic-dynamic conditions along each overpass or orbit. In order to assess the synoptic-dynamic state of the upper troposphere, the study makes use of two separate tracers for stratospheric influence: (1) low specific humidity and (2) enhanced potential vorticity.

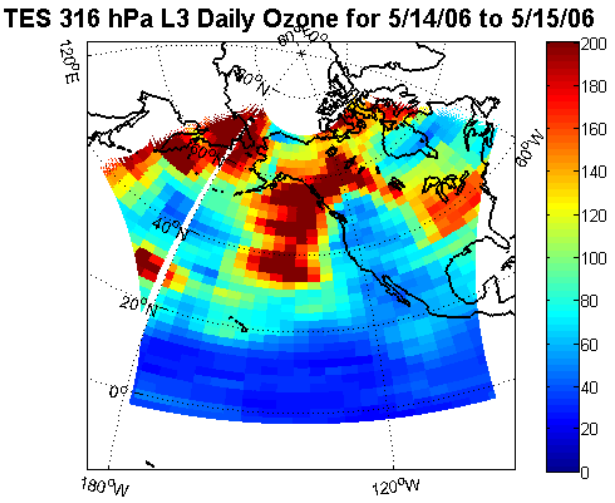

Fig. 1. TES Level 3 Daily Ozone plot for 14–15 May 2006 at 316 hPa. Images such as this are an example of what is currently available in terms of quick-view map products of UT ozone from TES.

Research has shown that the amount of water vapor present in the upper troposphere can be used to determine regions of stratospheric influence (Gray et al., 1994). Since water vapor mixing ratios are extremely low in the stratosphere and high within the planetary boundary layer, regions of the upper troposphere which exhibit very low water vapor mixing ratios are most often the result of downward vertical motion and exchange from the stratosphere. Regions which exhibit relatively high water vapor mixing ratios are most often the result of upward vertical motion and exchange from the boundary layer or lower free troposphere. Furthermore, a series of studies have shown that high-magnitude specific humidity gradients in the UT correspond to the location of the tropopause break and associated regions of aircraft observed stratosphere-troposphere exchange (Wimmers and Moody, 2001, 2004a,b; Wimmers et al., 2003).

Traditionally, potential vorticity (PV) is used as a tracer for air of stratospheric origin in the upper troposphere (Ancellet et al., 1994; Beuermann et al., 2002; Stohl et al., 2003; Pan et al., 2007). PV is both a thermodynamic and a dynamic quantity; it is the product of two terms, (1) atmospheric static stability which is a measure of the vertical potential temperature gradient, and (2) the fluid circulation or absolute vorticity, which is a measure of horizontal changes in wind velocity (speed or directional shear). PV increases rapidly in the lower stratosphere due almost entirely to the static stability component. Conserved under adiabatic conditions, as air moves from the stratosphere to UT, it carries the signature

of enhanced PV. Strong gradients in UT water vapor, PV and ozone help delineate the jet stream, the polar tropopause break and the large scale synoptic features of UT ridges and troughs as the flow moves poleward and equatorward, at times forming filamentary meridional streamers. While Langrangian contour advection methods preserve the filamentary nature of potential vorticity, Eulerian models do not always capture these finely scaled features, or they can be displaced in space and time by model error. However, the filamentation and fragmentation of stratospheric intrusions have long been recognized in satellite water vapor imagery (Appenzeller and Davies, 1992; Bader et al., 1995; Liniger and Davies, 2003).

1.2 Previous satellite-based tropospheric ozone measurements

Previous satellite systems have been used to derive tropospheric column residual ozone from polar orbiting platforms based on total ozone columns (e.g., from the Total Ozone Mapping Spectrometer, TOMS) and stratospheric profiles from solar backscattered ultraviolet (SBUV) measurements or more recently stratospheric columns from microwave limb soundings (MLS). The residual method requires accurate stratospheric observations and until the launch of the Aura satellite, collocated stratospheric and tropospheric columns were not available. Early methods relied upon TOMS total column ozone and derived the stratospheric column from the Stratospheric Aerosol and Gas Experiment II (Fishman and Larsen, 1987; Fishman et al., 1990), while later work has been based upon stratospheric profiles from SBUV (Fishman et al., 2003) or stratospheric columns from Upper Atmosphere Research Satellite (UARS) Microwave Limb Sounder (MLS) (Chandra et al., 2003).

After the launch of the Aura Earth Observing System, collocated stratospheric and tropospheric columns were available from OMI and the microwave limb sounder, MLS (Ziemke et al., 2006). More recent work by Schoeberl et al. (2007) expanded the domain of the stratospheric columns by using high resolution trajectories to advect the stratospheric features and increase the number of coincident measurements. While the seasonality of month-to-month estimates of tropospheric ozone residual (TOR) matched tropospheric columns calculated from ozonesondes, it was found that the method did not perform as well on daily time scales, or in the extratropics (Ziemke et al., 2006). This was improved upon in the results reported by Schoeberl et al. (2007), which found higher correlations and lower standard deviations when comparing OMI and trajectory mapped MLS total columns of tropospheric ozone residual (TOR) with ozonesondes; furthermore, they showed TES tropospheric columns could also be used to validate the derived TOR. Again, similar to Ziemke, while Schoeberl et al. (2007) found reasonable agreement in the midladitudes, they found that there was better agreement with ozonesondes in the tropics. The authors attributed this to the fact that MLS, with lower precision in the lower stratosphere, does not effectively resolve steep ozone gradients in the vicinity of the midlatitude tropospause.

The work presented in this paper was pursued to address the ability of a multi-sensor satellite approach to resolve variations in extratropical ozone on a daily (or better) time scale. We show that TES in the upper-troposphere does effectively capture sharp horizontal gradients in the mid-latitude troposphere that correspond to the location of the polar-tropopause break and associated STE. Furthermore, we illustrate that specific meteorological conditions of high PV and low specific humidity occur along with the TES ozone enhancements in STE preferred regions; regions like the eastern North Pacific mid-latitudes as identified in previous analyses of satellite derived total column ozone by Chandra et al. (2004) during spring months of 2000 and 2001. In this way, our work represents a step forward in using satellite observations to map the dynamic behavior of tropospheric ozone.

1.3 Research objective and motivations

The NASA INTEX-B program involved an extensive field campaign over the North Pacific during the spring of 2006. A main focus of the campaign was analysis of ozone and ozone precursor transport from Eastern Asia to the west coast of North America (Singh et al., 2006). Independent ozone measurements were made over the North American portion of the study region with ozonesondes during the INTEX Ozonesonde Network Study 2006 (IONS06), (Thompson et al., 2007a,b), while in situ FASTOZ aircraft measurements and DIAL curtains were made along flight tracks out of Hawaii and Anchorage (NASA DC-8) and in situ ozone was measured onboard the NCAR C-130 flying out of Seattle. During the field campaign, TES special observation retrievals were planned to coincide with sonde launches and aircraft ascents/descents. This paper has two objectives. The first is to demonstrate the ability of TES to observe synoptic-dynamic variation in upper tropospheric ozone. This is a largely qualitative assessment. The second is to derive a quantitative correlation between TES-observed UT ozone and synoptic-dynamical tracers in order to produce statistical retrievals of layer-averaged UT ozone across the entire INTEX-B study region.

The motivations for this work are as follows: (1) the need for integrative studies which make use of geostationary imagery to expand the coverage and provide context for polar-orbiting observations like AURA TES ozone, (2) the value of mapping natural background ozone levels in the free troposphere in order to more accurately characterize anthropogenic pollution transport (as in INTEX-B), (3) the need for greater knowledge of the spatial distribution of UT ozone as a function of time in order to assess clear-sky radiative forcing impacts, (4) the need for a synoptic-dynamic perspective when examining temporal changes in atmospheric ozone.

2 Data sets

2.1 GOES layer average specific humidity fields

GOES Layer Average Specific Humidity (GLASH) is a derived-product image of upper-tropospheric specific humidity based on the Geostationary Operational Environmental Satellites (GOES) Imager 6.7 micron water vapor absorption channel (Moody et al., 1999). By demonstrating that the 6.7 micron channel brightness temperatures respond to variations in specific humidity, atmospheric temperature, and satellite viewing angle, Wimmers and Moody (2001) were able to retrieve an image that shows only the contribution from layer average specific humidity by removing the variation in brightness temperature due to zenith angle and atmospheric temperature. The vertical sensitivity of the GLASH product is defined by the vertical contribution weighting function, which exhibits maximum sensitivity at 400 hPa and contribution weighting between 500 hPa and 300 hPa. High GLASH brightness values correspond to high water vapor mixing ratios in the mid-to-upper troposphere, while low brightness values likewise correspond to low water vapor mixing ratios in the same layer. The GOES-West domain was chosen to correspond to the study area of the INTEX-B program. GLASH fields were produced from 16 April 2006 to 16 May 2006 at intervals of 6 h (00:00, 06:00, 12:00, and 18:00 UTC) covering the majority of the INTEX-B study.

2.2 GFS model potential vorticity fields

The Global Forecast System (GFS) is an operational global numerical weather prediction model. This study makes use of GFS analysis (0 h forecast) grids and GFS calculation of potential vorticity (PV) from model temperature and wind fields. The GFS fields used in this study have a horizontal resolution of 1 degree by 1 degree with 26 vertical levels, at 50 hPa intervals in the troposphere. GFS model PV was calculated throughout the INTEX-B time period (from 16 April to 16 May 2006) at 6 h intervals corresponding in time with the GLASH products (00:00, 06:00, 12:00, and 18:00 UTC). To achieve spatial correspondence with GLASH as well, only GFS PV data within the GOES-West domain were used in this study.

2.3 TES special observation step and stare ozone profiles

TES special observation products known as nadir step and stare (SS) observations were performed throughout the INTEX-B time period. Every SS atmospheric curtain consists of 125 nadir column ozone measurements along the Aura satellite track, with each retrieved profile separated from its neighbor by ∼45 km (Osterman et al., 2007). The latitude range of the TES SS curtains corresponds well with the GOES-West latitude domain, with measurements from 15 degrees north to 65 degrees north. TES ozone profiles are calculated using an optimal estimation approach based on contemporaneous temperature, water vapor, and ozone retrievals from TES (Rodgers, 2000; Worden et al., 2004; Bowman et al., 2002, 2006) and a priori values based on a climatology from the Model of Ozone and Related Chemical Tracers (MOZART).

3 Methodology

The concept behind the multi-sensor UT ozone product (MUTOP) derived in this study is similar in its methodology to the EUMETSAT Multi-sensor Precipitation Estimate (MPE) product (Heinemannet al., 2002). This MPE product is a blending of geostationary IR retrievals with microwave sensors on polar-orbiting satellites through statistical correlation. The utility of the product is based on its high temporal and spatial resolution (geostationary component) and improved accuracy (polar-orbiting component). This logic of blending the advantages of polar and geostationary remote sensing platforms (Aura TES and GOES GLASH) is at the core of the MUTOP product.

3.1 Averaging of equivalent atmospheric layers between data sets

In order to assess the correlation between TES ozone and the dynamical tracers (specific humidity and PV), it was first necessary to layer average the three data sets such that all three are representative of the same general layer within the atmosphere. A contribution weighting function interpolated to match GLASH was applied to TES ozone measurements in the upper troposphere as shown below:

$$\begin{aligned}\overline{\mathrm{TES\,O_3}} = \{&0.128\times[(\mathrm{OZ_{287}}+\mathrm{OZ_{316}})/2]+0.204\times\mathrm{OZ_{348}}\\ &+0.256\times[(\mathrm{OZ_{383}}+\mathrm{OZ_{422}})/2]+0.242\\ &\times\mathrm{OZ_{464}}+0.169\times\mathrm{OZ_{511}}\}\end{aligned} \quad (1)$$

The notation $\mathrm{OZ_{287}}$, refers to TES-retrieval of ozone at 287 hPa, etc., for each of the levels used in the average. The layer averaging was chosen to represent the majority of the peak of the GLASH contribution weighting function while eliminating excess weighting in the stratosphere. This results in average TES ozone (and GFS PV) which correspond to the atmospheric layer of highest weighting for the GLASH product. Therefore any further references to the upper troposphere (UT) in this paper will specifically refer to the atmospheric layer from 500 to 300 hPa, peaking at 400 hPa (see Fig. 2 for an example of the TES ozone and GFS PV averaged layer).

3.2 Regression analysis

Multivariate regression analysis was used to determine the statistical correlation between layer-average TES ozone measurements, layer-average GFS model PV estimates, and

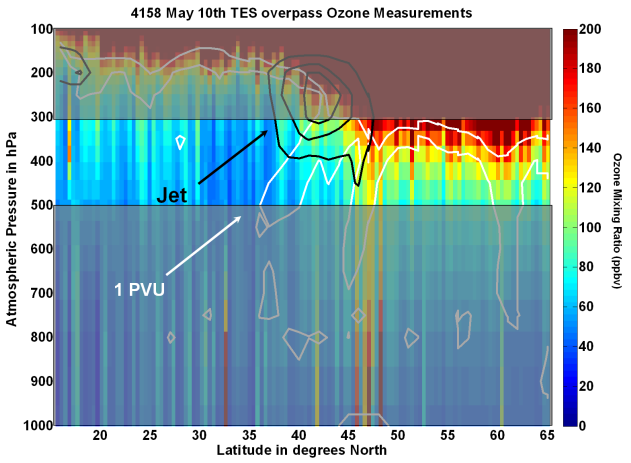

Fig. 2. Plot of TES "Step and Stare" ozone profile curtain for 10 May 2006, in which the ozone volume mixing ratio (VMR) is plotted in color shading (ppbv). The location of the jet stream (black contours) and of the 1 and 3 PV-unit contours (white) are also plotted to show the dynamical context (both from GFS model). The vertical extent of layer-averaging for TES ozone and GFS PV is designated by the black outline (500 to 300 hPa).

layer-average specific humidity (i.e., GLASH brightness value retrievals). To prepare the data for regression analysis, each TES ozone measurement was matched to its spatially-closest GLASH brightness value and GFS PV counterparts. Since the GFS model resolution is significantly lower than that of TES nadir retrievals, in many cases more than one layer-average TES ozone value was matched with the same PV value along an AURA orbit track.

Because this study is concerned with the impact of synoptic dynamics on upper tropospheric ozone, it was important to make sure that excessive error from a lack of temporal coincidence did not make its way into the data set. Since GLASH products and GFS model fields were available at 6 h intervals, the greatest possible time separation for TES overpasses from one of these fields was 3 h. To reduce the error from time separation and the potential for sampling entirely different air masses as features move, a temporal coincidence criterion of 1.5 h was established for the regression data sets. Although this could still result in some error in comparison, it is a tighter coincidence requirement than has been used in previous TES validation studies (Nassar et al., 2008; Richards et al., 2008; Worden et al., 2007b).

Based on these criteria, the final data set consists of 30 TES Step and Stare curtains over the North Pacific and within the GOES-West domain. These 30 TES cross-sections contain 3134 individual vertical profiles, and the same number of individual layer-average TES ozone measurements. In order to set aside cases for error evaluation, the data set was randomly split into a training data set (75 %, or 2351 values), and an evaluation data set (25 %, or 783 values). A multiple linear regression was performed on the training data, with TES layer-average ozone as the dependent variable and GLASH brightness values and GFS layer-average PV as the independent variables.

$$\overline{\mathrm{TESO_3}} = \mathrm{a} \times \mathrm{GLASH} + \mathrm{b} \times \overline{\mathrm{PV}} + \mathrm{c} \quad (2)$$

The over-bar symbol implies the UT layer average, and will be assumed in all further reference to TES and PV. The regression analysis provides a statistical model of the correlation between TES ozone and the synoptic dynamical tracers (GOES GLASH and GFS PV) where all three were observed along the TES orbit and yields a statistical retrieval method for estimating ozone over the rest of the GOES-West domain. In order to evaluate the derived product, the regression equation from the training data set was applied to the GOES GLASH and GFS PV values from the remaining 25 % of the data set, creating a comparison of predicted multi-sensor layer-average upper tropospheric ozone values (MUTOP) versus observed (TES), and a providing a measure of model error.

4 Results

4.1 Case study evaluations

Simple visual analysis of GOES GLASH and GFS PV fields with TES UT ozone overlays (Fig. 3), demonstrate that TES upper troposphere layer average ozone retrievals clearly do respond to dynamical variations in the UT. As can be seen in these images, TES-observed ozone is elevated in and around the edges of upper-level troughs, in dry-air streamers, and in cut-off lows (which correspond with low water vapor and high GFS PV values). This same correspondence was observed for all of the TES overpasses which occurred during the INTEX-B period and fell within the GOES-West domain.

Figure 3 also shows the great amount of variation in the TES observed ozone between orbits, and illustrates the influence of meteorological conditions. In the first overpass (13 May at 12:00 UTC), TES measurements follow the trough axis and generally display two distinct UT ozone regimes: the southern portion observed air with relatively low (40–60 ppbv) UT ozone and the northern portion within the upper level low, found considerable stratospheric influence and elevated UT ozone (120–200 ppbv). This situation is not unexpected, and fits well with the climatological mean within the Northern Hemisphere mid-latitudes during spring. In the second overpass (14 May, 00:00 UTC), the TES instrument observed the very western edge of the same trough feature that it passed through 12 h earlier. In this case, TES measured slightly heightened UT ozone mixing ratios along the western edge of the trough (100 ppbv), then transitioned back into a warm, moist, ozone poor UT within the upper-level ridge (40–60 ppbv). In the last example (15 May at 12:00 UTC), TES observed a climatological anomaly and

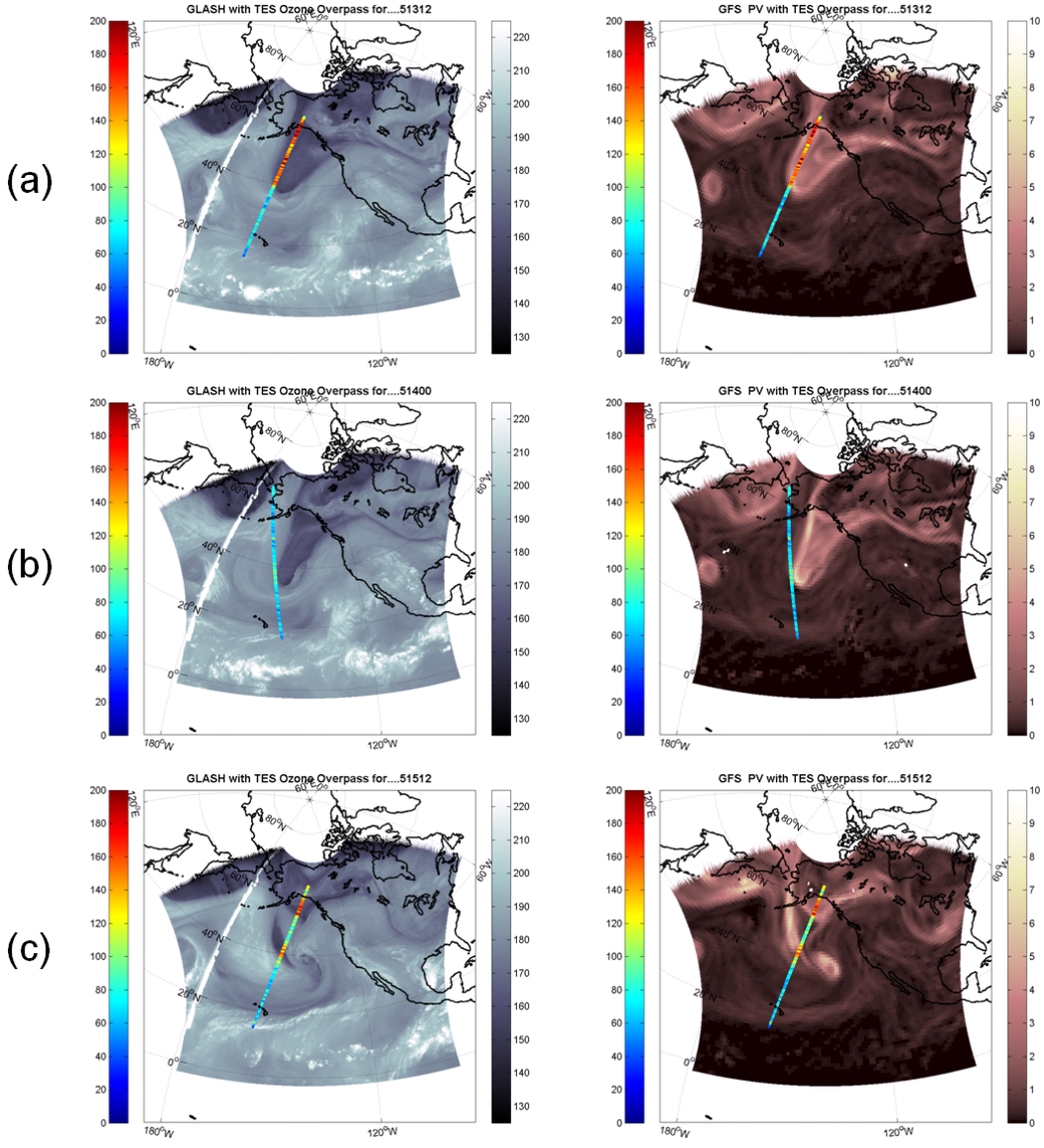

Fig. 3. This set of plots shows individual TES overpass layer-average UT ozone VMR (color shaded in ppbv) plotted over fields of GLASH BV (grey shading) and GFS PV (pink shading in PV units) for three different times (**(a)** 13 May at 12:00 UTC, **(b)** 14 May at 00:00 UTC, and **(c)** 15 May at 12:00 UTC). Note the strong negative correlation between TES UT ozone and GLASH BV and the strong positive correlation between TES UT ozone and GFS PV.

still captured the dynamical variation in UT ozone quite well. By this time, the upper-level trough observed during the previous orbits had evolved and a distinct cut-off low formed at its base. Moving generally from south to north, TES first observed moist, free tropospheric air with little ozone present in the UT (60 ppbv). It then encountered the western side of the cut-off low feature, where TES observed heightened UT ozone mixing ratios (120–160 ppbv), corresponding with strong signatures of atmospheric aridity and high PV. Ozone mixing ratios decreased on the northern side of the cut-off low, in the vicinity of recently mixed moist, relatively low PV air (60–80 ppbv) before increasing again as TES passed over the remnants of the original upper-level trough (120–180 ppbv).

4.2 Regression results

Based on the relationship between layer-average TES ozone and the two tracers, the following multiple linear regression was derived from the training dataset (see Fig. 4 for regression plot):

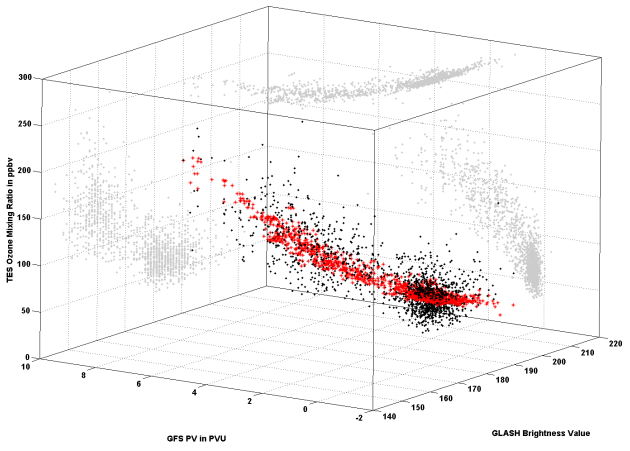

Fig. 4. 3-D plot of layer average UT ozone (as observed by TES) vs. corresponding GLASH brightness value and layer average UT GFS PV value. Observations are plotted as black dots, while predicted regression values (multiple-linear in the form of a plane) are plotted in red. Observations are projected (in light grey) on to each axis for easier interpretation.

$$\text{TES\_O}_3 = -1.21\,\text{ppbv} \times \text{GLASH} + 17.05\,\text{ppbv} \times \text{PV} + 281.4\text{ppbv} \quad (3)$$

Table 1 summarizes the results, illustrating that 72 % of the variance in TES layer average ozone can be explained by the multiple-linear regression, with an error of 18 ppbv. Because atmospheric aridity and potential vorticity are in fact inversely correlated (the GLASH versus PV correlation coefficient is -0.71), we have also addressed the issue of collinearity which has the potential to cause instability in the regression coefficients (a and b in Table 1). Our results suggest this is not a problem. Table 1 shows errors in the regression coefficients are all on the order of 3 %. The tolerance is a measure of the unexplained variance (50 %) *between the regression variables*. A variance inflation factor (the inverse of tolerance) on the order of 10 would suggest collinearity.

While the GOES Layer Average Specific Humidity (GLASH) brightness values and the GFS PV are inversely correlated ($r = -0.71$ in the training dataset), we believe they each add content which is unique in explaining the variability in ozone. The variables were considered separately to evaluate their capacity to explain variation in TES observed ozone. The authors recognize that while PV has traditionally been used as an effective tracer, when operating over data sparse regions like the North Pacific, the model may have errors of magnitude or displacement of features. Indeed, it was the original goal of this project to try to define an empirical and independent method for extrapolating the information that TES provides to a larger domain, based on a correlation of remotely sensed information from two satellite platforms. However, it was found that individually GLASH could explain 60 % of the variance in TES, with a standard error of 22 ppbv. So a purely satellite-based product was not very effective. Furthermore, the residuals of this regression indicated the largest errors in estimating TES ozone occur for high ozone values. Similarly, variability in PV alone could explain 63 % of the variance in TES ozone, with a standard error of 21ppbv. The use of both variables together in a multiple regression was able to increase the explained variance and reduce the residual error. In fact, the two independent variables provide complimentary power, with specific humidity explaining more of the variance in ozone in lower PV air while PV explains more of the variance in ozone in very dry air.

To produce ozone imagery at the GOES resolution, the training data regression equation was applied to all of the GLASH and PV data, every six hours, across the GOES-West domain. All the MUTOP images presented in this paper are based on the regression equation calculated from the training data set (75 % of the TES data). A statistical comparison of the MUTOP product to the TES *evaluation data* (the reserved 25 % of data not used in deriving the regression), resulted in the following relationship, summarized in Table 2:

$$\text{TES\_O}_3 = 1.02 \times \text{MUTOP} \quad (4)$$

Figure 5 displays the overall correlation between TES UT ozone and MUTOP modeled values, as well as the distribution of MUTOP residuals for the evaluation data set. The mean absolute error (MAE) and root mean square error (RMSE) were 13.6 ppbv and 18.1 ppbv for the predicted versus observed ozone. These errors are comparable to the RMSE of 17.8 to 21.9 ppbv in the TES validation study reported by Nassar et al. (2008) when comparing TES UT ozone to ozonesondes at latitudes from 15 to 90 degrees north. Given the overall observed TES_O_3 range from 30 ppbv to 230 ppbv, these results suggest the MUTOP product provides a decent representation of TES measurements, with a slight bias toward under-representation of high UT ozone values and over-representation of low UT ozone values.

4.3 Statistical retrieval ozone products

The regression results were used to create a statistical retrieval of MUTOP, the Multi-sensor layer-average UT Ozone Product (MUTOP) at six hour intervals for the entire INTEX-B time period (see Fig. 6 and the Supplement animation link). There are several advantages to the MUTOP derived image product: (1) calculated from fields (GLASH and GFS PV) that can be produced operationally, it can be created and used in near real-time to diagnose the distribution and forecast the movement of UT ozone; (2) it provides good coverage (at GOES water vapor channel spatial resolution) on the distribution of dynamically driven ozone in the UT; (3) created at 6 h intervals, it provides a sub-daily visualization of the rapid movement of dynamically-driven ozone in the UT.

Table 1. Multiple regression and error analysis results from using GLASH and PV together to explain variance in the dependent variable of TES observed ozone in the UT, based on the training data set (75 % of data) . Collinearity tests evaluate the independence of the predictors.

Model Parameters	Coefficient	Standard Error	Significance[a]	Collinearity Tolerance	Variance Inflation
Constant	281.40	7.99	.000		
a	−1.21	.04	.000	0.50	2.0
b	17.05	.54	.000	0.50	2.0
R^2	0.72	18.47	.000		

[a] probability of two-tailed t-test, $p < .001$ is highly significant

Table 2. Analysis of MUTOP (predicted from regression described in Table 1) against TES (observed), for the 25 % of data held in reserve for evaluation (considers TES to be dependent variable).

Model Parameters	Coefficient	Standard Error	Significance [a]
Constant	−1.13	1.97	.57
a	1.02	.02	.000
R^2	0.73	18.14	.000

[a] probability of two-tailed t-test, $p < .001$ is highly significant

5 Discussion

5.1 Product performance and utility

Regression analysis shows that over 70 % of variation in upper tropospheric ozone (as observed by TES) can be explained by the synoptic dynamic tracers of UT specific humidity (GLASH) and potential vorticity (GFS PV) during spring 2006 within the GOES-West domain. This finding suggests that ozone variability in the UT is predominantly controlled by dynamical processes, with some of the scatter likely explained by systematic errors such as temporal and parallax displacement, model error, and resolution/interpolation artifacts. However, other factors not included in the MUTOP model, such as in situ chemical production/destruction of ozone and long-range transport of ozone from polluted boundary layers, are certainly important influences on UT ozone as well. As part of the 2003 Intercontinental Transport and Chemical Transformation (ITCT 2K2) study, for example, Cooper et al. (2004b) addressed the capacity of warm conveyor belt systems as transporters of polluted boundary layer air from the Asian continent into the North Pacific mid-and-upper troposphere. They found that 44 % of warm conveyor belt air masses drew their chemical composition from a lower troposphere source, leading to heightened ozone mixing ratios in warm conveyor belts over the North Pacific. These findings may help to explain limited MUTOP performance under moist, low PV conditions,

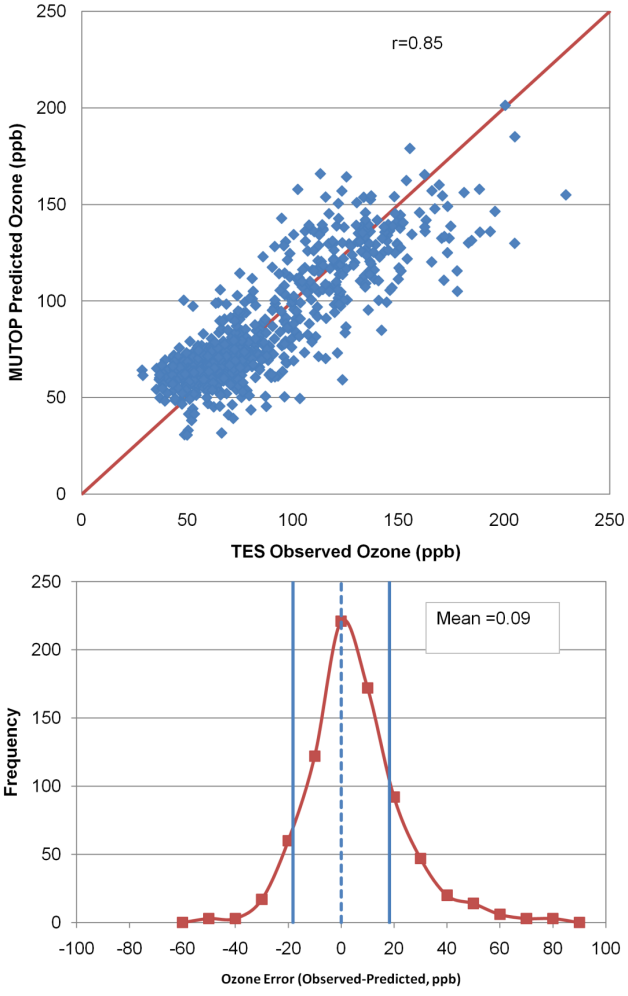

Fig. 5. Comparison between TES and MUTOP ozone estimates. The upper panel shows the correlation, and the solid line displays a perfect model one-to-one relationship for comparison. The lower panel shows the probability density function of the difference between TES and MUTOP, with the average denoted by the dashed line, and the standard deviation by the solid lines.

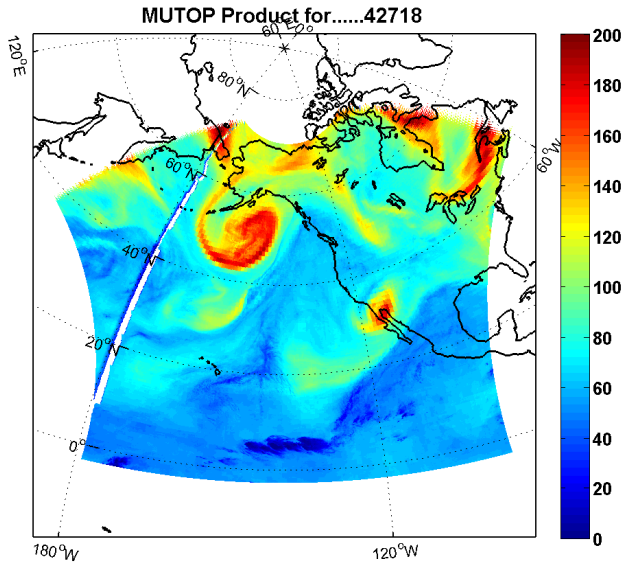

Fig. 6. Example MUTOP retrieval from 27 April 2006 at 18:00 UTC depicting ozone across the GOES-West domain. Upper tropospheric layer-average ozone mixing ratio is shaded in color in ppbv.

as warm conveyor belt air masses and subtropical free tropospheric air masses may have similar tracer characteristics (enhanced specific humidity and low PV), but could display very divergent ozone chemistries. Overall, the MUTOP product is not as effective at characterizing ozone mixing ratio variability within moist air masses; synoptic dynamics have less control on UT ozone mixing ratios in these regions. However, the results of this study are supportive of the conclusions of Cooper et al. (2004a,b), which found upper tropospheric dynamics can result in the transport of stratospheric ozone enhancements into the lower troposphere under the right synoptic conditions.

Although MUTOP has limitations as noted above, it provides a capacity for upper tropospheric ozone estimation within the GOES domain that is a large step beyond what is currently available in the form of spatially-derived daily ozone plots based on TES retrievals alone (Fig. 7). This figure shows what was previously available in the form of a TES-derived "daily" ozone product within the GOES-West domain (bottom right of panel) in comparison to five panels of corresponding images produced from the method described in this paper. The previously available image is a TES Level 3 Daily Ozone plot for 24 April 2006. This particular image was created by averaging the 464 hPa and 316 hPa plots. The Level 3 product at each of these specific pressure levels is created by combining TES global survey overpass measurements from a 26 h period (in this case from ∼12:00 UTC on the 24th to ∼12:00 UTC on the 25th) and spatially interpolating between overpass measurements.

Although the TES Level 3 Daily Ozone is useful as a browse product for identification of regions of interest for further research and investigation, they are limited in several ways with regard to accurate synoptic- and meso-scale dynamical representation of ozone in the upper troposphere. First, the Aura satellite and the TES instrument are in sun-synchronous polar orbit, meaning that the satellite moves retrograde from east to west. This is opposite the movement of most large-scale weather systems in the Northern Hemisphere mid-latitudes, and thus L3 ozone products may distort synoptic features in the UT. Second, the L3 product is presented as a daily plot, but the measurements used in interpolations that are spatially proximate can be from entirely different times of day (ascending and descending nodes). Therefore the L3 products do not represent a simple daily mean, but instead provide a stitched-together representation of UT ozone from different times during a 26 h period. As a result UT ozone enhancements associated with small-scale features that fall between overpasses (e.g., meridional streamers) may be completely missed, and any features that are not continuous between overpasses may be incorrectly characterized in the spatial averaging.

A comparison of five MUTOP images corresponding to the 26 h interval over which the one TES Level 3 Daily Ozone map is stitched together is provided in Fig. 7. Here one can see that MUTOP provides greater meteorological context for UT ozone observations than has been available previously in these L3 products. MUTOP, at 6 h temporal resolution, identifies coherent synoptic and mesoscale features in the UT which are either missed or poorly resolved in the L3 products. For example, from the 24–25 April case in Fig. 7, the L3 product fails to capture specific features in the UT, such as in the elongated streamer just off the Pacific Northwest and California coastlines. The disadvantage of spatial interpolation becomes evident, as can be seen in the L3 product's poor characterization of two distinct ozone enhancements over Eastern Canada in Fig. 7. The TES L3 Daily plot suggests that these features are connected; MUTOP sees the distinction between them in terms of dynamics. Once the separate panels of the multi-sensor product are viewed, it is much easier to understand the features coarsely rendered in the TES L3 product. Overall, MUTOP allows for better interpretation of individual TES overpasses and associated Level 3 Daily Ozone plots and clearly demonstrates an improvement in UT ozone characterization over the GOES-West domain.

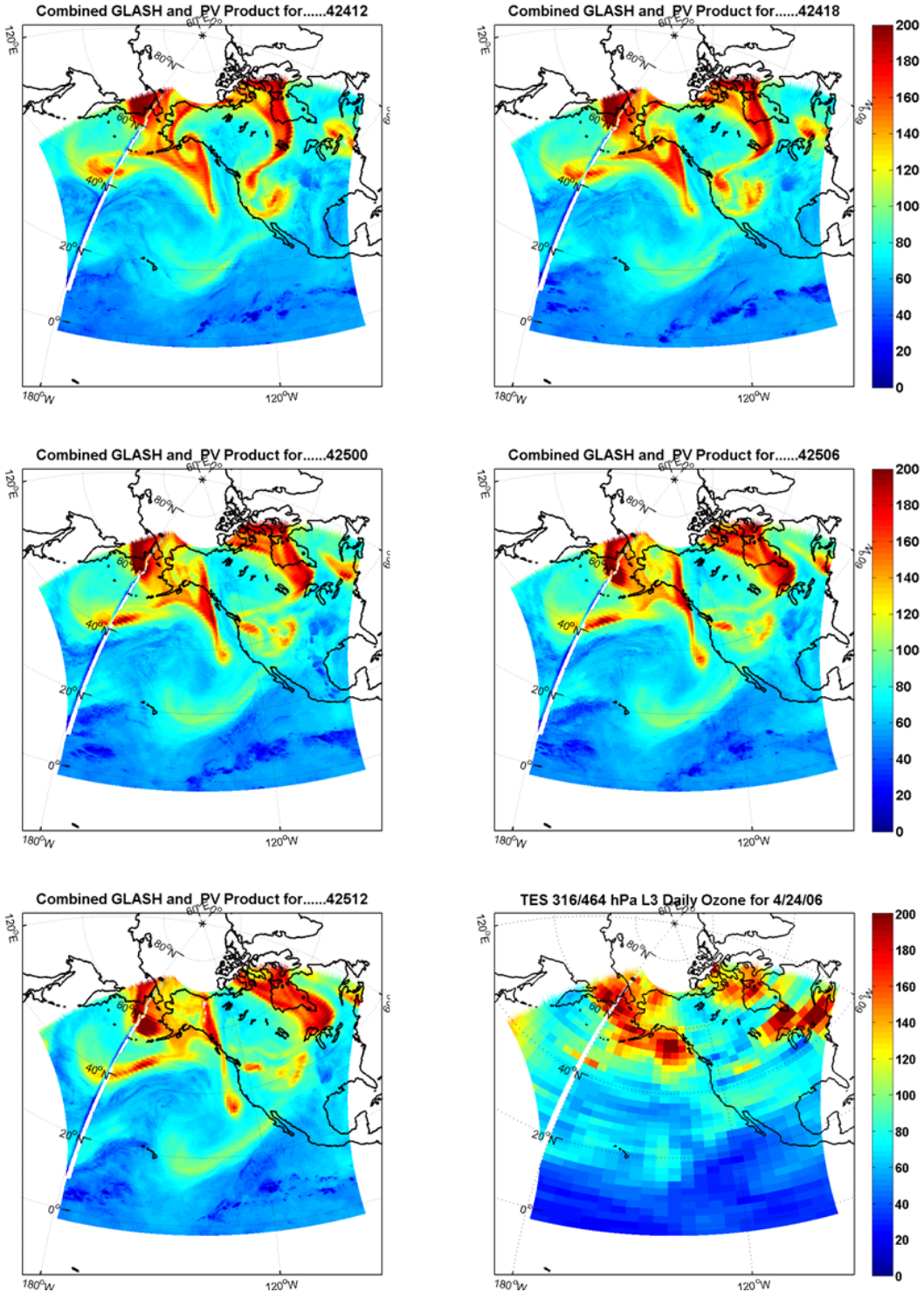

Fig. 7. Plot of 5 (first 5 panes) MUTOP products from the at 6 h intervals from 24 April at 12:00 UTC to 25 April at 12:00 UTC. These images correspond to the time over which TES global survey overpass measurements were used to create the TES Level 3 Daily Ozone plot (bottom right pane) through spatial interpolation. This daily ozone plot is an average of the 316 and 464 hPa daily plots for that day (to better match the UT ozone plots). Ozone mixing ratio is plotted in color in all panes in ppbv.

6 Conclusions and recommendations for future work

MUTOP provides a dynamic meteorological context for transient ozone enhancements and helps to illustrate the overall highly variable ozone mixing ratios in the UT. With relatively high spatial and temporal resolution, MUTOP derived imagery allows for viewing even mesoscale dynamical features (dry air streamers and cut-off lows) *and their evolution* through image looping. MUTOP provides visualization of UT ozone that surpasses what is currently available in the form of TES Level 3 Daily Ozone maps. Tropospheric ozone estimates are also available based on the extraction of tropospheric residuals from satellite total column ozone measurements, as noted earlier (Sect. 1.2). Another residual technique presented by Yang et al. (2007) used PV mapping to increase the resolution of the stratospheric column estimate for deriving TOR. Yang used the correlation between MLS ozone and potential vorticity in the lower stratosphere to provide a higher spatial resolution stratospheric column, which yielded improvements in the midlatitude TOR estimates. In general, it has been shown by all of these TOR methods that the ozone gradients in the residual often correspond with gradients in the heights of the tropopause, and these change with synoptic conditions in the midlatitudes. The MUTOP product is complimentary to satellite derived TOR results, but has the advantage of providing higher resolution sub-daily depictions of ozone in the extratropics, where the TOR method was less effective.

This work demonstrates gradients in TES ozone are strongly correlated with remotely sensed aridity and modeled PV, and provides a method for mapping the significant springtime ozone variability in the upper troposphere driven by dynamics and stratospheric exchange, at the resolution of a geostationary satellite. In order to establish the legitimacy of the product derivation, independent validation of MUTOP has been carried out against ozonesonde measurements from the INTEX-B campaign within the GOES-West domain. This validation also provides an indirect assessment of TES UT ozone retrieval, since MUTOP estimates are derived from the TES-tracer relationship. A subsequent paper describes this work in detail and compares MUTOP validation results to those of past TES validation studies (Moody et al., 2011).

Overall, the satellite derived product of layer-average UT ozone, or MUTOP, represents the TES retrieval of UT ozone during the INTEX-B campaign reasonably well; however, there are some limitations which could be addressed through further study. First, the derived regression should be tested for periods other than spring before application to different seasons, in order to assess robustness. Since STE is believed to be at a maximum in the northern mid-latitudes during spring, the current regression relationship may lead to overestimates in other seasons (Appenzeller et al., 1996). Second, the regression relationships could be tested over the same spring period in other years in order to evaluate its robustness with respect to inter-annual variation in UT ozone (Thouret et al., 2006). Finally, it might be beneficial to assess the correlation between high-magnitude regression residuals and a tracer for anthropogenic pollution such as CO, to inform our understanding of the large degree of scatter around the regression model.

Supplementary material related to this article is available online at: http://www.atmos-chem-phys.net/11/6515/2011/acp-11-6515-2011-supplement.zip.

Acknowledgements. UVA participation in the INTEX/B field program was supported by NASA (award NNG06GA93G). We thank the UCAR Unidata program for data access to near real-time GOES imagery.

Edited by: M. Van Roozendael

References

Ancellet, G., Beekmann, M., and Papayannis, A.: Impact of a cutoff low development on downward transport of ozone in the troposphere, J. Geophys. Res.-Atmos., 99, 3451–3468, 1994.

Appenzeller, C. and Davies, H. C.: Structure of stratospheric intrusions into the troposphere, Nature, 358, 570–572, 1992.

Appenzeller, C., Holton, J. R., and Rosenlof, K. H.,: Seasonal variation of mass transport across the tropopause, J. Geophys. Res., 101, 15071–15078, 1996.

Bader, J. J., Forbes, G. S., Grant, J. R., Lilley, R. B. E., and Waters, A. J. (Eds): Images in Weather Forecasting: A Practical Guide for Interpreting Satellite and Radar Imagery, Cambridge Univ. Press, New York, USA, 1995.

Beer, R.: TES on the Aura Mission: Scientific Objectives, Measurements, and Analysis Overview, IEEE T. Geosci. Remote, 44, 1102–1105, 2006.

Beer, R., Glavich, T. A., and Rider, D. M.: Tropospheric emission spectrometer for the Earth Observing System's Aura satellite, Appl. Opt., 40(15), 2356–2367, doi:10.1364/AO.40.002356, 2001.

Beuermann, R., Konopka, P., Brunner, D., Bujok, O., Gunther, G., McKenna, D. S., Lelieveld, J., Muller, R., and Schiller, C.: High-resolution measurements and simulation of stratospheric and tropospheric intrusions in the vicinity of the polar jet stream, Geophys. Res. Lett., 29, 1577, doi:10.1029/2001gl014162, 2002.

Bowman, K. W., Worden, J., Steck, T., Worden, H. M., Clough, S., and Rodgers, C.: Capturing time and vertical variability of tropospheric ozone: A study using tes nadir retrievals, J. Geophys. Res.-Atmos., 107, 4723, doi:10.1029/2002jd002150, 2002.

Bowman, K. W., Rodgers, C. D., Kulawik, S. S., Worden, J., Sarkissian, E., Osterman, G., Steck, T., Lou, M., Eldering, A., Shephard, M., Worden, H., Lampel, M., Clough, S., Brown, P., Rinsland, C., Gunson, M., and Beer, R.: Tropospheric emission spectrometer: Retrieval method and error analysis, IEEE T. Geosci. Remote, 44, 1297–1307, doi:10.1109/TGRS.2006.871234, 2006.

Bowman, K. P., Pan, L. L., Campos, T., and Gao, R.: Observations of fine-scale transport structure in the upper troposphere from the high-performance instrumented airborne platform for environmental research, J. Geophys. Res.-Atmos., 112, D18111, doi:10.1029/2007jd008685, 2007.

Chandra, S., Ziemke, J. R., and Martin, R. V.: Tropospheric ozone at tropical and middle latitudes derived from TOMS/MLS residual: Comparison with a global model, J. Geophys. Res., 108(D9), 4291, doi:10.1029/2002JD002912, 2003.

Cooper, O., Forster, C., Parrish, D., Dunlea, E., Hubler, G., Fehsenfeld, F., Holloway, J., Oltmans, S., Johnson, B., Wimmers, A., and Horowitz, L.: On the life cycle of a stratospheric intrusion and its dispersion into polluted warm conveyor belts, J. Geophys. Res.-Atmos., 109, D23s09, doi:10.1029/2003jd004006, 2004a.

Cooper, O. R., Forster, C., Parrish, D., Trainer, M., Dunlea, E., Ryerson, T., Hubler, G., Fehsenfeld, F., Nicks, D., Holloway, J., de Gouw, J., Warneke, C., Roberts, J. M., Flocke, F., and Moody, J.: A case study of transpacific warm conveyor belt transport: Influence of merging airstreams on trace gas import to north america, J. Geophys. Res.-Atmos., 109, D23s08, doi:10.1029/2003jd003624, 2004b.

Fairlie, T. D., Avery, M. A., Pierce, R. B., Al-Saadi, J., Dibb, J., and Sachse, G.: Impact of multiscale dynamical processes and mixing on the chemical composition of the upper troposphere and lower stratosphere during the intercontinental chemical transport experiment-north america, J. Geophys. Res.-Atmos., 112, D16s90, doi:10.1029/2006jd007923, 2007.

Gauss, M., Myhre, G., Pitari, G., Prather, M. J., Isaksen, I. S. A., Berntsen, T. K., Brasseur, G. P., Dentener, F. J., Derwent, R. G., Hauglustaine, D. A., Horowitz, L. W., Jacob, D. J., Johnson, M., Law, K. S., Mickley, L. J., Muller, J. F., Plantevin, P. H., Pyle, J. A., Rogers, H. L., Stevenson, D. S., Sundet, J. K., van Weele, M., and Wild, O.: Radiative forcing in the 21st century due to ozone changes in the troposphere and the lower stratosphere, J. Geophys. Res.-Atmos., 108, 4292, doi:10.1029/2002jd002624, 2003.

Fishman, J. and Larsen, J. C.: Distribution of total ozone and stratospheric ozone in the tropics: Implications for the distribution of tropospheric ozone, J. Geophys. Res., 92(D6), 6627–6634, doi:10.1029/JD092iD06p06627, 1987.

Fishman, J., Watson, C. E., Larsen, J. C., and Logan, J. A.: Distributionof tropospheric ozone determined from satellite data, J. Geophys. Res., 95(D4), 3599–3617, 1990.

Fishman, J., Wozniak, A. E., and Creilson, J. K.: Global distribution of tropospheric ozone from satellite measurements using the empirically corrected tropospheric ozone residual technique: Identification of the regional aspects of air pollution, Atmos. Chem. Phys., 3, 893–907, doi:10.5194/acp-3-893-2003, 2003.

Gray, L. J., Bithell, M., and Cox, B. D.: The role of specific-humidity fields in the diagnosis of stratosphere troposphere exchange, Geophys. Res. Lett., 21, 2103–2106, 1994.

Heinemann, T., Lattanzio, A., and Roveda, F.: The EUMETSAT Multi-sensor Precipitation Estimate (MPE), http://www.eumetsat.int/groups/ops/documents/document/mpe{_}introduction{_}ipwg{_}2002.pdf, 2002.

Hilsenrath, E., Schoeberl, M. R., Douglass, A. R., Bhartia, P. K., Barnett, J., Beer, R., Waters, J., Gunson, M., Froidevaux, L., Gille, J., and Levelt, P. F.: Early data from aura and continuity from uars and toms, Space Sci Rev, 125, 417–430, doi:10.1007/s11214-006-9074-1, 2006.

Hudman, R. C., Jacob, D. J., Cooper, O. R., Evans, M. J., Heald, C. L., Park, R. J., Fehsenfeld, F., Flocke, F., Holloway, J., Hubler, G., Kita, K., Koike, M., Kondo, Y., Neuman, A., Nowak, J., Oltmans, S., Parrish, D., Roberts, J. M., and Ryerson, T.: Ozone production in transpacific asian pollution plumes and implications for ozone air quality in california, J. Geophys. Res.-Atmos., 109, D23s10, doi:10.1029/2004jd004974, 2004.

Liniger, M. A. and Davies, H. C.: Substructure of a MAP Streamer, Q .J. R. Meteorol. Soc., 129, 633–651, doi:10.1256/qj.02.28, 2003.

Moody, J. L., Felker, S. R., Wimmers, A. J., Osterman, G. Bowman, K., Thompson, A. M., and Tarasick, D. W.: A Multi-sensor Upper Tropospheric Ozone Product (MUTOP) based on TES Ozone and GOES Water Vapor: Validation with Ozonesondes, submitted, Atmos. Chem. Phys., 2011.

Nassar, R., Logan, J. A., Worden, H. M., Megretskaia, I. A., Bowman, K. W., Osterman, G. B., Thompson, A. M., Tarasick, D. W., Austin, S., Claude, H., Dubey, M. K., Hocking, W. K., Johnson, B. J., Joseph, E., Merrill, J., Morris, G. A.,Newchurch, M., Oltmans, S. J., Posny, F., Schmidlin, F. J., Vomel, H., Whiteman, D. N., and Whitte, J.C.: Validation of Tropospheric Emission Spectrometer (TES) nadir ozone profiles using ozonesonde measurements, J. Geophys. Res., 113, D15S17, doi:10.1029/2007JD008819, 2008.

Osterman, G. B. (Ed.): Tropospheric Emission Spectrometer TES L2 Data User's Guide, version 3.00, Jet Propulsion Laboratory, California Institute of Technology, Pasadena, CA, USA, 2007.

Pan, L. L., Bowman, K. P., Shapiro, M., Randel, W. J., Gao, R. S., Campos, T., Davis, C., Schauffler, S., Ridley, B. A., Wei, J. C., and Barnet, C.: Chemical behavior of the tropopause observed during the Stratosphere-Troposphere Analyses of the Regional Transport experiment, J. Geophys. Res., 112, D18110, doi:10.1029/2007JD008645, 2007.

Richards, N. A. D., Osterman, G. B., Browell, E. V., Hair, J. W., Avery, M., and Li, Q. B.: Validation of tropospheric emission spectrometer ozone profiles with aircraft observations during the intercontinental chemical transport experiment-b, J. Geophys. Res.-Atmos., 113, D16s29, doi:10.1029/2007jd008815, 2008.

Rodgers, C. D. and Connor, B. J.: Intercomparison of remote sounding instruments, J. Geophys. Res.-Atmos., 108, 4116, doi:10.1029/2002jd002299, 2003.

Shepherd, T. G.: Issues in stratosphere-troposphere coupling, J. Meteorol. Soc. Jpn., 80, 769–792, 2002.

Schoeberl, M. R., Ziemke, J. R., Bojkov, B., Livesey, N., Duncan, B., Strahan, S., Froidevaux, L., Kulawik, S., Bhartia, P. K., Chandra, S., Levelt, P. F., Witte, J. C., Thompson, A. M., Cuevas, E., Redondas, A., Tarasick, D. W., Davies, J., Bodeker, G., Hansen, G., Johnson, B. J., Oltmans, S. J., Vomel, H., Allaart, M., Kelder, H., Newchurch, M., Godin-Beekmann, S., Ancellet, G., Claude, H., Andersen, S. B., Kyro, E., Parrondos, M., Yela, M., Zablocki, G., Moore, D., Dier, H., von der Gathen, P., Viatte, P., Stubi, R., Calpini, B., Skrivankova, P., Dorokhov, V., de Backer, H., Schmidlin, F. J., Coetzee, G., Fujiwara, M., Thouret, V., Posny, F., Morris, G., Merrill, J., Leong, C. P., Koenig-Langlo, G., and Joseph, E.: A trajectory-based estimate of the tropospheric ozone column using the residual method, J. Geophys. Res.-Atmos., 112, D24s49, doi:10.1029/2007JD008773, 2007.

Singh, H. B., Brune, W. H., Crawford, J. H., Fuelberg, H., and

Jacob, D. J.: The Intercontinental Chemical Transport Experiment – Phase B (INTEX-B): An update, http://www.espo.nasa.gov/docs/intex-b/INTEX-B_WhitePaper.pdf, 2006.

Stohl, A., Bonasoni, P., Cristofanelli, P., Collins, W., Feichter, J., Frank, A., Forster, C., Gerasopoulos, E., Gaggeler, H., James, P., Kentarchos, T., Kromp-Kolb, H., Kruger, B., Land, C., Meloen, J., Papayannis, A., Priller, A., Seibert, P., Sprenger, M., Roelofs, G. J., Scheel, H. E., Schnabel, C., Siegmund, P., Tobler, L., Trickl, T., Wernli, H., Wirth, V., Zanis, P., and Zerefos, C.: Stratosphere-troposphere exchange: A review, and what we have learned from staccato, J. Geophys. Res.-Atmos., 108, 8516, doi:10.1029/2002jd002490, 2003.

Tarasick, D. W., Moran, M. D., Thompson, A. M., Carey-Smith, T., Rochon, Y., Bouchet, V. S., Gong, W., Makar, P. A., Stroud, C., Menard, S., Crevier, L. P., Cousineau, S., Pudykiewicz, J. A., Kallaur, A., Moffet, R., Menard, R., Robichaud, A., Cooper, O. R., Oltmans, S. J., Witte, J. C., Forbes, G., Johnson, B. J., Merrill, J., Moody, J. L., Morris, G., Newchurch, M. J., Schmidlin, F. J., and Joseph, E.: Comparison of canadian air quality forecast models with tropospheric ozone profile measurements above midlatitude north america during the ions/icartt campaign: Evidence for stratospheric input, J. Geophys. Res.-Atmos., 112, D12s22, doi:10.1029/2006jd007782, 2007.

Thompson, A. M., Stone, J. B., Witte, J. C., Miller, S. K., Oltmans, S. J., Kucsera, T. L., Ross, K. L., Pickering, K. E., Merrill, J. T., Forbes, G., Tarasick, D. W., Joseph, E., Schmidlin, F. J., McMillan, W. W., Warner, J., Hintsa, E. J., and Johnson, J. E.: Intercontinental chemical transport experiment ozonesonde network study (ions) 2004: 2. Tropospheric ozone budgets and variability over northeastern north america, J. Geophys. Res.-Atmos., 112, D12s13, doi:10.1029/2006jd007670, 2007a.

Thompson, A. M., Stone, J. B., Witte, J. C., Miller, S. K., Pierce, R. B., Chatfield, R. B., Oltmans, S. J., Cooper, O. R., Loucks, A. L., Taubman, B. F., Johnson, B. J., Joseph, E., Kucsera, T. L., Merrill, J. T., Morris, G. A., Hersey, S., Forbes, G., Newchurch, M. J., Schmidlin, F. J., Tarasick, D. W., Thouret, V., and Cammas, J. P.: Intercontinental chemical transport experiment ozonesonde network study (ions) 2004: 1. Summertime upper troposphere/lower stratosphere ozone over northeastern north america, J. Geophys. Res.-Atmos., 112, D12s12, doi:10.1029/2006jd007441, 2007b.

Thouret, V., Cammas, J.-P., Sauvage, B., Athier, G., Zbinden, R., Nédélec, P., Simon, P., and Karcher, F.: Tropopause referenced ozone climatology and inter-annual variability (1994-2003) from the MOZAIC programme, Atmos. Chem. Phys., 6, 1033–1051, doi:10.5194/acp-6-1033-2006, 2006.

Wang, W. C., Liang, X. Z., Dudek, M. P., Pollard, D., and Thompson, S. L.: Atmospheric ozone as a climate gas, Atmos. Res., 37, 247–256, 1995.

Wimmers, A. J. and Moody, J. L.: A fixed-layer estimation of upper tropospheric specific humidity from the GOES water vapor channel: Parameterization and validation of the altered brightness temperature product, J. Geophys. Res.-Atmos., 106, 17115–17132, 2001.

Wimmers, A. J., Moody, J. L., Browell, E. V., Hair, J. W., Grant, W. B., Butler, C. F., Fenn, M. A., Schmidt, C. C., Li, J., and Ridley, B. A.: Signatures of tropopause folding in satellite imagery, J. Geophys. Res.-Atmos., 108, 8360, doi:10.1029/2001jd001358, 2003.

Wimmers, A. J. and Moody, J. L.: Tropopause folding at satellite-observed spatial gradients: 1. Verification of an empirical relationship, J. Geophys. Res.-Atmos., 109, D19306, doi:10.1029/2003jd004145, 2004a.

Wimmers, A. J. and Moody, J. L.: Tropopause folding at satellite-observed spatial gradients: 2. Development of an empirical model, J. Geophys. Res.-Atmos., 109, D19307, doi:10.1029/2003jd004146, 2004b.

Worden, H. M., Bowman, K. W., Worden, J. R., and Eldering, A.: TES observations of tropospheric ozone as a greenhouse gas, (Poster) Eos Trans. AGU, 88(52), Fall Meet. Suppl., A51D–0735, 2007a.

Worden, H. M., Logan, J. A., Worden, J. R., Beer, R., Bowman, K., Clough, S. A., Eldering, A., Fisher, B. M., Gunson, M. R., Herman, R. L., Kulawik, S. S., Lampel, M. C., Luo, M., Megretskaia, I. A., Osterman, G. B., and Shephard, M. W.: Comparisons of tropospheric emission spectrometer (tes) ozone profiles to ozonesondes: Methods and initial results, J. Geophys. Res.-Atmos., 112, D03309, doi:10.1029/2006jd007258, 2007b.

Worden, J., Kulawik, S. S., Shephard, M. W., Clough, S. A., Worden, H., Bowman, K., and Goldman, A.: Predicted errors of tropospheric emission spectrometer nadir retrievals from spectral window selection, J. Geophys. Res.-Atmos., 109, D09308, doi:10.1029/2004jd004522, 2004.

Yang, Q., Cunnold, D.M., Wang, H.-J, Froidevaux, L., Claude, H., Merrill, J., Newchurch, M., and Oltmans, S.J.: Midlatitude tropospheric ozone columns derived from the Aura Ozone Monitoring Instrument and Microwave Limb Sounder measurements, J. Geophys. Res.-Atmos,. 112, D20305, doi:10.1029/2007JD008528, 2007.

Ziemke, J. R., Chandra, S., Dunca, B. N., Froidevaux, L., Bhartia, P. K., Levelt, P. F., and Waters, J. W.: Tropospheric ozone determined from Aura OMI and MLS: Evaluation of measurements and comparison with the Global Modeling Initiative's Chemical Transport Model, J. Geophys. Res.-Atmos., 111, D19303, doi:10.1029/2006JD007089, 2006.